Molecular Imaging
Volume 16: 1-7

DOI: 10.1177/1536012117736703
journals.sagepub.com/home/mix
SAGE

Effect of Time-of-Flight and Regularized Reconstructions on Quantitative Measurements and Qualitative Assessments in Newly Diagnosed Prostate Cancer With ^{18}F-Fluorocholine Dual Time Point PET/MRI

Spencer C. Behr, MD[1], Brett J. Mollard, MD[1,2], Jaewon Yang, PhD[1], Robert R. Flavell, MD, PhD[1], Randall A. Hawkins, MD, PhD[1], and Youngho Seo, PhD[1,3]

Abstract

Recent technical advances in positron emission tomography/magnetic resonance imaging (PET/MRI) technology allow much improved time-of-flight (TOF) and regularized iterative PET reconstruction regularized iterative reconstruction (RIR) algorithms. We evaluated the effect of TOF and RIR on standardized uptake values (maximum and peak SUV [SUV_{max} and SUV_{peak}]) and their metabolic tumor volume dependencies and visual image quality for ^{18}F-fluorocholine PET/MRI in patients with newly diagnosed prostate cancer. Fourteen patients were administered with 3 MBq/kg of ^{18}F-fluorocholine and scanned dynamically for 30 minutes. Positron emission tomography images were divided to early and late time points (1-6 minutes summed and 7-30 minutes summed). The values of the different SUVs were documented for dominant PET-avid lesions, and metabolic tumor volume was estimated using a 50% isocontour and SUV threshold of 2.5. Image quality was assessed via visual acuity scoring (VAS). We found that incorporation of TOF or RIR increased lesion SUVs. The lesion to background ratio was not improved by TOF reconstruction, while RIR improved the lesion to background ratio significantly ($P < .05$). The values of the different VAS were all significantly higher ($P < .05$) for RIR images over TOF, RIR over non-TOF, and TOF over non-TOF. In conclusion, our data indicate that TOF or RIR should be incorporated into current protocols when available.

Keywords

cancer detection imaging, novel imaging methods/agents for clinical studies, quantitation in molecular imaging, cancer imaging, PET/MRI, prostate cancer

Introduction

Prostate cancer remains the most common cancer diagnosed in men in the United States and is among the leading causes of cancer-related mortality.[1] Imaging continues to play an increasing role in the evaluation of prostate cancer and suspected cancer recurrence. Multiparametric prostate magnetic resonance imaging (MRI) is the current diagnostic imaging workhorse, although it is still undergoing continuous evolution to overcome inherent limitations. For example, Muller et al recently showed that the revised Prostate Imaging Reporting and Data System (PI-RADS 2.0) provides moderately reproducible MRI scores similar to PI-RADS 1.0 for clinically relevant prostate cancer.[2] Newer experimental radiopharmaceuticals have made positron emission tomography (PET) combined

[1] Department of Radiology and Biomedical Imaging, University of California, San Francisco, San Francisco, CA, USA
[2] TRA-MINW, PS, Tacoma, WA, USA
[3] Department of Radiation Oncology, University of California, San Francisco, San Francisco, CA, USA

Submitted: 30/06/2017. Revised: 14/08/2017. Accepted: 10/09/2017.

Corresponding Authors:
Youngho Seo, UCSF Physics Research Laboratory, San Francisco, CA 94107, USA.
Spencer C. Behr, Department of Radiology and Biomedical Imaging, UCSF, San Francisco, CA, USA.
Emails: youngho.seo@ucsf.edu; spencer.behr@ucsf.edu

with computed tomography (CT) and MRI interesting research subjects aimed at improving the diagnostic accuracy of prostate cancer diagnosis.[3-5]

Combined with multiparametric prostate MRI, PET imaging in PET/MRI is a natural extension of current prostate imaging practice.[6,7] Recent advancements in PET detector technology also have made time-of-flight (TOF) imaging capability and its associated TOF-enabled reconstruction, which is a standard technology in modern PET/CT scanners, feasible in the clinical PET/MRI setting. The TOF-enabled reconstruction (hereinafter, "TOF reconstruction" for simplicity) is known for improved spatial resolution, contrast to noise ratio, and image quality in PET/CT.[8-13] The improved resolution for TOF reconstruction, in comparison to that for non-TOF reconstruction (ie, the reconstruction without the TOF feature), is primarily due to faster convergence; thus at comparable iterations, TOF reconstruction typically yields better spatial resolution than non-TOF reconstruction does.

Further technological advance in TOF-PET, particularly the use of solid-state photomultipliers instead of photomultiplier tubes as the photodetector, made it possible for the TOF capability to be implemented even in a strong magnetic field, translating it into clinical PET/MRI systems as well.[12,14-16]

In addition to TOF reconstruction capability, a regularized iterative reconstruction (RIR) algorithm has been clinically implemented (Q.Clear; GE Healthcare, Waukesha, Wisconsin).[17-20] However, this regularized reconstruction algorithm has not been available clinically for PET/MRI yet. Currently, no literature exists examining the effect of TOF or regularized reconstruction on standardized uptake values (SUVs), image quality, or lesion conspicuity for PET/MR imaging of prostate cancer. Also, there is no standard static acquisition protocol for the clinically used prostate cancer PET radiopharmaceuticals such as ^{11}C-acetate, ^{18}F-fluorocholine, and ^{68}Ga-labelled Glu-urea-Lys(Ahx)-HBED-CC (68Ga–HBED-CC).[3-5,21] We acquired our ^{18}F-fluorocholine PET/MRI dynamically over 30 minutes, so that we could evaluate the performance of static acquisitions by summing early and late imaging time (dual-time) points.

In this report, we compared effects of dual-time point imaging and TOF and RIR techniques on lesion maximum and peak SUV (SUV_{max} and SUV_{peak}), background pelvic mean SUV (SUV_{mean}), metabolic tumor volume estimated by PET using a 50% isocontour boundary, visual image quality assessment, and confidence in lesion detection in the evaluation of newly diagnosed biopsy-proven high-risk prostate cancer with non-TOF ordered subsets expectation maximization (OS-EM) reconstruction.

Materials and Methods

Patient Cohort

From April 1, 2015, until October 30, 2015, 14 men (average age of 62 years $\pm$ 7) diagnosed with biopsy-proven intermediate or high-grade prostate cancer characterized by preoperative Cancer of the Prostate Risk Assessment (CAPRA) score[22,23] (ie, CAPRA score $\geq$ 3) were evaluated with ^{18}F-fluorocholine PET/MRI of the pelvis in this institutional review board–approved study. Dominant clinically relevant tumors with Gleason score 3+4/4+3 or greater were evaluated. Prostatic lesions were found in 12 patients, and a total of 17 tumors were identified by ^{18}F-fluorocholine PET/MRI for quantitative analysis.

^{18}F-Fluorocholine PET/MRI Protocol

Positron emission tomography imaging was performed immediately following intravenous (IV) administration of 3 MBq/kg of ^{18}F-fluorocholine via a peripheral IV catheter after at least 4 hours of fasting for 30 minutes. Positron emission tomography images were acquired on a TOF-PET/3-tesla MRI scanner (SIGNA PET/MR; GE Healthcare) in 3-D acquisition mode over the pelvis. ^{18}F-fluorocholine uptake was recorded in list mode and the list -mode data were replayed into 2 time points, 1 to 6 minutes summed and 7 to 30 minutes summed after administration of the radiotracer. Based on the observation of the tracer kinetics over 30 minutes from dynamic reconstructions of the entire 30 minutes,[16] the early time duration (1-6 minutes), excluding the first minute of mostly blood pool uptake, was determined since the rapid uptake of ^{18}F-fluorocholine reaches a plateau mostly around 5 to 6 minutes. In addition, the late time duration (7-30 minutes), with at least a minute gap from the early time point, was determined to capture accumulated activity after the radiotracer reached the plateau. Reconstruction was performed in a matrix size of 128 $\times$ 128 (voxel size = 2.34 $\times$ 2.34 $\times$ 2.78 mm^3) with other parameters: transverse field of view = 300 mm, TOF-enabled and TOF-disabled OS-EM algorithm with 28 subsets and 2 iterations, 5-mm full-width at half-maximum postreconstruction Gaussian filter and 1:4:1 axial filter for both TOF-enabled reconstruction ("TOF reconstruction"), and TOF-disabled reconstruction ("non-TOF reconstruction"). Finally, the RIR algorithm was used for the same data sets with a regularization parameter beta value of 350, 3 and 2 initial non-TOF regularized and OS-EM iterations followed by 8 TOF regularized iterations. A set of representative images using non-TOF, TOF, and RIR algorithms for both time points (early and late) are shown in Figure 1. The choice of reconstruction parameters such as the number of iterations, the number of subsets, and the sequence of non-TOF and TOF regularized iterations were based on the vendor-default recommended parameters which are commonly used at our center as well, not intended to be optimized further by our own investigation. This way, we assessed the image qualities from each reconstruction algorithm as all of the readers using this imaging system would see.

Magnetic resonance imaging was performed simultaneously during PET acquisition utilizing an endorectal coil. Standard MR-based attenuation correction was applied using liver accelerated volume acquisition -flex MR images (repetition time [TR] $\sim$ 4 millisecond, echo time [TE]: 2.23 millisecond, flip angle: 5° or 12° , partial Fourier: 70.3%, acquisition time: 18 seconds) with a standard body coil developed for PET/MRI

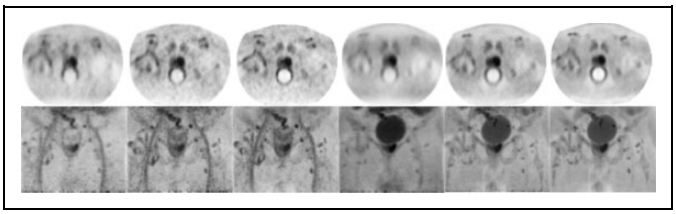

Figure 1. A representative set of images reconstructed using non-TOF, TOF, and RIR algorithms. Axial images are shown in the top row, and maximum intensity projection (MIP) images are shown in the bottom row. From left to right: non-TOF, TOF, and RIR images from the early (1-6 minute) time point data set. Non-TOF, TOF, and RIR images from the late (7-30 minute) time point data set. RIR indicates regularized iterative reconstruction; TOF, time-of-flight.

(lower anterior array coil; GE Healthcare). Axial T2-weighted with fat-saturation, axial diffusion-weighted imaging with *b* values = 0, 50, 600, and 1350, axial apparent diffusion coefficient maps, axial T1-weighted without and with fat saturation prior to gadolinium-based contrast (gadobutrol) administration, dynamic contrast-enhanced axial T1-weighted with fat saturation, and MR spectroscopy pulse sequences were obtained. Washin and washout curves were generated and mapped over the prostate. For this investigation of comparing different PET reconstructions, we did not use any of these MR images, by the way.

Positron Emission Tomography Image Analyses

All reconstructed PET images were reviewed independently by 2 board-certified radiologists with training in nuclear medicine. Maximum and peak SUVs[24] (SUV_{max} and SUV_{peak}) were documented for dominant suspicious prostate lesions and SUV_{mean} was obtained of the pelvis (ischium) as background. All SUVs were measured on OsiriX (Pixmeo, Bernex, Switzerland). Metabolic tumor volume by PET was measured using a 50% isocontour and an SUV threshold of 2.5 to determine tumor boundaries and calculate the encompassed volume utilizing OsiriX. For quantitative analysis, we first examined the difference in SUV measurements from different reconstruction for early (1-6 minutes) and late time (7-30 minutes) point data by taking the ratios of lesion SUV_{max} and SUV_{peak} from TOF and RIR reconstructions to those from non-TOF reconstructions.

Since an RIR reconstruction with a sufficiently large number of iterations results in a higher spatial resolution than corresponding TOF and non-TOF reconstructions, and a TOF reconstruction also converges faster than non-TOF reconstruction with the same number of iterations for both, the relative SUVs are expected to depend on the size of lesion where SUVs were derived. It is important to note that for RIR reconstruction, the number of iterations should be sufficiently large as in our case (3 and 2 initial non-TOF regularized and OS-EM iterations followed by 8 TOF regularized iterations) because RIR reconstruction can provide poorly converged images (ie, smoother images) accompanied by spatial resolution degradation. Hence, we also examined the lesion volume dependencies of these ratios by generating scatter plots of the ratios over the metabolic tumor volumes.

Then, we compared the lesion to background (target to background ratio or TBR) and lesion to blood ratios (target to blood or TBlood) from different reconstructions and different time point data to illustrate any perceived visual contrast of lesion to background with regard to different reconstruction and different time points. After this step, in order to depict how different reconstructions and different time points affect TBR and TBlood, we took ratios of TBRs and TBlood of TOF to those of non-TOF and ratios of TBRs and TBlood of RIR to those of non-TOF reconstructions for both time point (early and late) data sets. Finally, image quality was subjectively assessed using visual acuity scoring (VAS), ranking image quality on a scale of 1 to 100. The paired 2-tailed *t* test was used to compare the SUV ratios, TBRs, TBloods, and VAS's to investigate whether the difference is statistically significant.

Results

Standardized Uptake Values Consistency

Relative lesion SUVs for TOF and RIR data sets to non-TOF data sets ($SUV_{TOF}/SUV_{non\text{-}TOF}$, $SUV_{RIR}/SUV_{non\text{-}TOF}$) are as follows. The ratios of SUV_{max} for TOF to that for non-TOF were 1.14 $\pm$ 0.29 (range: 1.00-1.72) for the 1- to 6-minute uptake period and 1.17 $\pm$ 0.13 (range: 1.02-1.45) for the 7- to 30-minute uptake period, respectively. The ratios of SUV_{max} for RIR to that for non-TOF were 1.56 $\pm$ 0.42 (range: 1.20-2.64) for the 1- to 6-minute uptake period and 1.26 $\pm$ 0.42 (range: 1.00-2.43) for the 7- to 30-minute uptake period, respectively. The ratios of SUV_{peak} for TOF to that for non-TOF were 1.14 $\pm$ 0.13 (range: 0.98-1.49) for the 1- to 6-minute uptake period and 1.11 $\pm$ 0.10 (range: 0.93-1.30) for the 7- to 30-minute uptake period, respectively. The ratios of SUV_{peak} for RIR to that for non-TOF were 1.30 $\pm$ 0.21 (range: 0.97-1.96) for the 1- to 6-minute uptake period and 1.06 $\pm$ 0.20 (range: 0.70-1.52) for the 7- to 30-minute uptake period, respectively. Figure 2 shows the SUV ratios for all reconstructions and at the 2 time points in 1 plot to depict the relative consistencies of SUV measurements. The relative lesion SUVs of RIR to non-TOF reconstructions are significantly larger than those of TOF to non-TOF in the early time point images ($P < .05$); however, the relative lesion SUVs of RIR to non-TOF reconstruction do not show statistically significant differences to those of TOF to non-TOF reconstruction in the late time point images ($P > .05$).

Standardized Uptake Values Dependence on Metabolic Volume

Using the metabolic volume average from 2 methods (50% isocontour and 2.5 SUV threshold) measured for the data sets reconstructed with TOF and RIR, scatter plots were generated to show the ratios of lesion SUVs (SUV_{max} and SUV_{peak}) of TOF to non-TOF and RIR to non-TOF reconstructions,

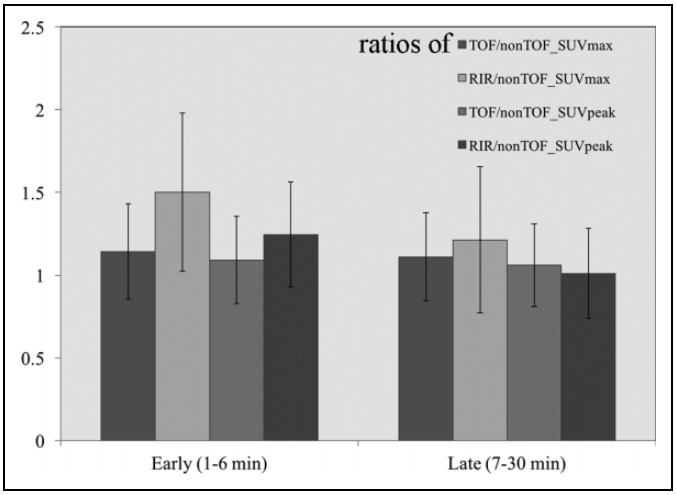

Figure 2. Ratios of SUV_{max} and SUV_{peak} in lesions of TOF to non-TOF and RIR to non-TOF reconstructions for the early (1-6 minutes summed) and late (7-30 minutes summed) data sets. RIR indicates regularized iterative reconstruction; SUV, standardized uptake values; TOF, time-of-flight.

respectively (Figure 3). These scatter plots clearly show the dependence on the measured volume for the relative SUVs. The smaller the metabolic tumor volume is, the larger relative SUVs were observed for both TOF and RIR reconstructions over non-TOF reconstructions. In addition, for the RIR reconstructions as they are expected to have better convergences than both TOF and non-TOF reconstructions, the difference in SUVs is greater in small metabolic volumes. These data also show that when the metabolic tumor size reaches approximately 4 mL, the relative SUVs do not show increase over the volume.

Lesion to Background and Lesion to Blood

Relative TBRs for TOF and RIR data sets to non-TOF data sets ($TBR_{TOF}/TBR_{non\text{-}TOF}$, $TBR_{RIR}/TBR_{non\text{-}TOF}$) and relative TBloods for TOF and RIR data sets to non-TOF data sets ($TBlood_{TOF}/TBlood_{non\text{-}TOF}$, $TBlood_{RIR}/TBlood_{non\text{-}TOF}$) are as follows. The ratios of TBR for TOF to that for non-TOF were 0.86 $\pm$ 0.25 (range: 0.59-1.47) for the 1- to 6-minute uptake period and 0.85 $\pm$ 0.13 (range: 0.54-1.02) for the 7- to 30-minute uptake period, respectively. The ratios of TBR for RIR to that for non-TOF were 1.03 $\pm$ 0.35 (range: 0.59-1.89) for the 1- to 6-minute uptake period and 1.04 $\pm$ 0.31 (range: 0.64-1.58) for the 7- to 30-minute uptake period, respectively. The ratios of TBlood for TOF to that for non-TOF were 0.96 $\pm$ 0.14 (range: 0.75-1.19) for the 1- to 6-minute uptake period and 1.07 $\pm$ 0.12 (range: 0.83-1.20) for the 7- to 30-minute uptake period, respectively. The ratios of TBlood for RIR to that for non-TOF were 1.57 $\pm$ 0.44 (range: 0.78-2.37) for the 1- to 6-minute uptake period and 1.20 $\pm$ 0.33 (range: 0.77-2.01) for the 7- to 30-minute uptake period, respectively. Figure 4 shows the TBRs and TBloods for all reconstructions and at the 2 time points in 1 plot to depict the changes and consistencies of lesion to background and lesion to blood contrast. The relative TBRs and TBloods of RIR over non-TOF are all larger than those of TOF over non-TOF reconstructions at all time points. The differences are all statistically significant ($P < .05$) except for the difference between TBlood of RIR over non-TOF and TBlood of TOF over non-TOF for the 7- to 30-minute data set ($P > .05$).

Image Quality

Mean VAS was 57.6, 68.1, and 80.9 for non-TOF, TOF, and RIR reconstructions, respectively for one of the radiologists,

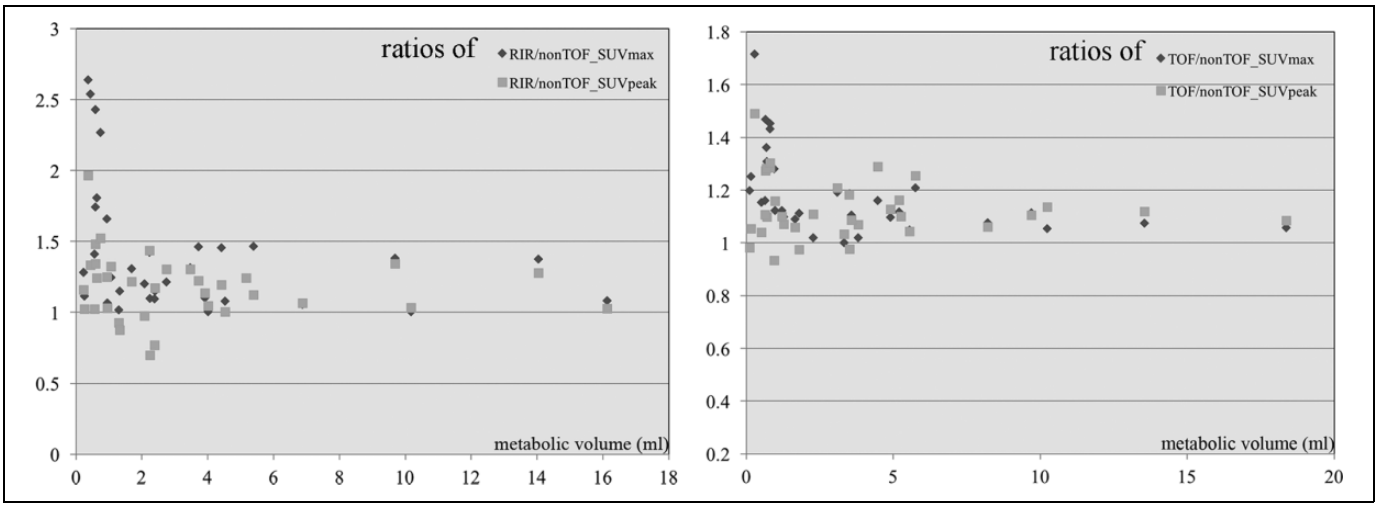

Figure 3. Scatter plots of SUVs (max and peak) measured from data sets reconstructed using the TOF and RIR algorithms over SUVs measured from data sets reconstructed using the non-TOF algorithm. RIR indicates regularized iterative reconstruction; SUVs, standardized uptake values; TOF, time-of-flight.

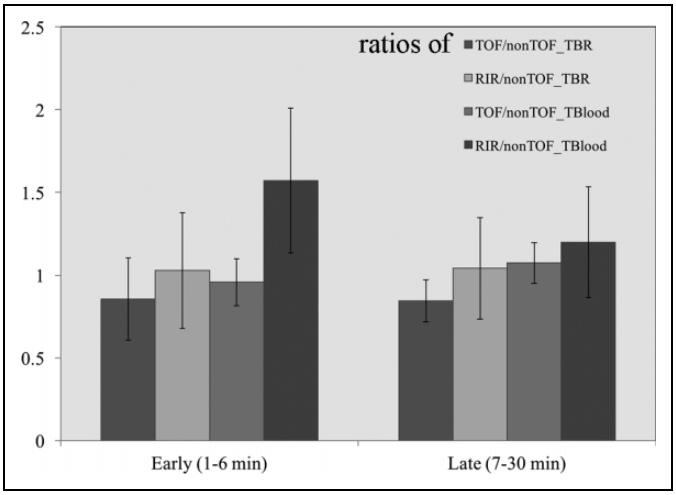

Figure 4. Target-to-background (TBR, lesion-to-ischium) and target-to-blood (TBlood, lesion-to-blood pool) differences are shown as ratios of TBRs and TBloods of TOF data sets to non-TOF data sets and RIR data sets to non-TOF data sets for both early and late time point images. RIR indicates regularized iterative reconstruction; TOF, time-of-flight.

and 58.8, 70.9, and 78.6, respectively, for the other radiologist for the 1- to 6-minute acquisition data sets and 48.4, 53.4, and 76.5, respectively, for one of the radiologists and 55.1, 68.4, and 75.4, respectively, for the other radiologist for the 7- to 30-minute acquisition data sets. The VAS was significantly higher for RIR reconstructed data sets over TOF reconstructed data sets, TOF over non-TOF, and RIR over TOF for both time point data sets ($P < .05$). The VAS was better for the early time point data (1-6 minutes summed) than the late time point data (7-30 minutes summed) for non-TOF reconstructions with statistical significance ($P < .05$) for both readers; however, for TOF and RIR reconstructions, there was no statistically significant difference ($P > .05$) between the 2 time point data. Figure 5 shows box plots of VAS between data sets for the 2 radiologists who performed VAS.

Discussion

Addition of TOF and RIR capability for image reconstruction to ^{18}F-fluorocholine PET/MRI increases SUV_{max} and SUV_{peak} for both 1- to 6-minute and 7- to 30-minute acquisition data sets over corresponding non-TOF data sets. The reason for this difference is primarily because of improved spatial resolution of TOF-enabled PET reconstruction when the same number of iterations was used in our case and improved spatial resolution of RIR PET reconstruction when a sufficient number of iterations were performed. Consistent with a modest increase in SUV_{max} and SUV_{peak} using TOF and RIR reconstructions, image quality assessed by VAS also showed significant improvement when TOF and regularized reconstructions were used over images generated by conventional non-TOF reconstructions. Some of these findings are in keeping with the previously reported benefits of TOF for PET/CT, including increased signal and contrast to noise ratio, improved lesion detectability, and detecting low contrast lesions in a noisy background by increasing sensitivity and reducing image noise.[9,25-27] These benefits of TOF should allow for a decrease in patient dose, acquisition time, or both as demonstrated following the addition of TOF to PET/CT.[28] Unlike extensive literature reports on the benefits of TOF reconstructions, reports of regularized reconstruction's benefits in quantitative measurements and qualitative visual image assessment using clinical data are scarce; however, our findings are consistent with a few case reports in the literature.[19,29]

There are several limitations inherent to this study, including small sample size and retrospective nature. Also, our assessment was only confined to prostate ^{18}F-fluorocholine PET/MRI data sets, while the TOF and RIR algorithms can be used for any other PET data sets when these algorithms are available. Effects of TOF and RIR on clinical outcomes and sensitivity of detecting intermediate or high-grade prostate cancer were not assessed. While radiotracer uptake was noted in all

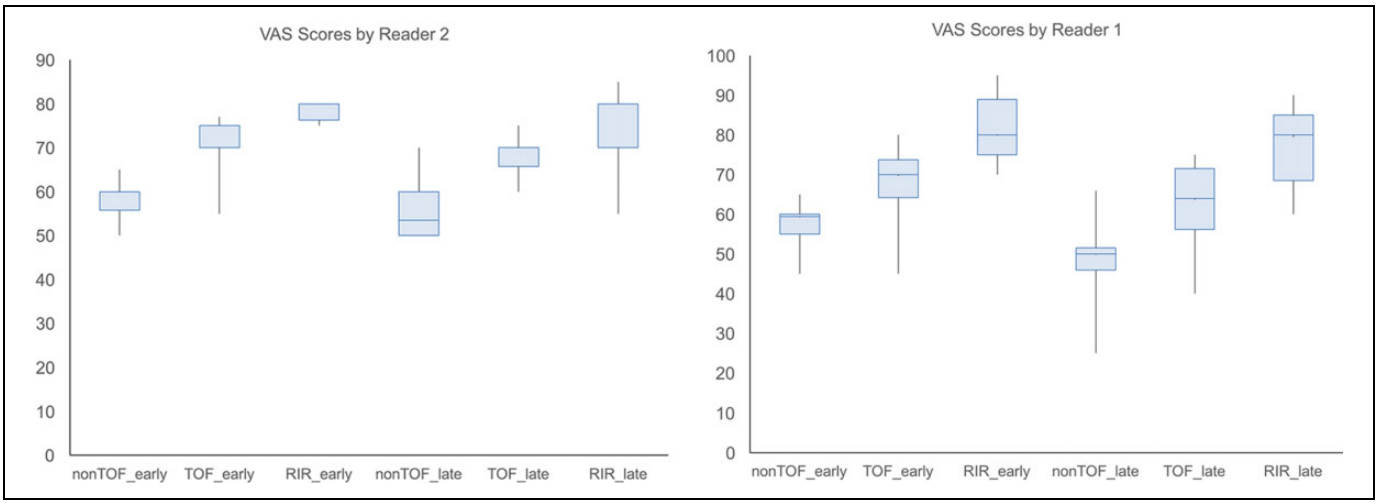

Figure 5. Box plots of VAS performed by 2 board-certified radiologists. VAS indicates visual acuity scoring.

lesions, uptake pattern in nontarget lesions, such as benign prostatic hypertrophy nodules, was not assessed. It is possible that the increase in SUV_{max} and SUV_{peak} with TOF and RIR could translate into an increased sensitivity in detecting small lesions, though this topic requires further investigation.

Conclusion

Our data strongly suggest that incorporation of TOF and RIR algorithms should be used when available for prostate ^{18}F-fluorocholine PET/MRI. In particular, RIR algorithm outperformed TOF algorithm without regularization when compared side-by-side in terms of image quality assessment for our data sets. Hence, in order to fully capture the promise of RIR algorithms, further investigation on the performance of RIR including TOF for other PET imaging scenarios is warranted.

Acknowledgments

We gratefully acknowledge Vahid Ravanfar for technical assistance to acquire and initially process all clinical PET imaging data.

Declaration of Conflicting Interests

The author(s) declared no potential conflicts of interest with respect to the research, authorship, and/or publication of this article.

Funding

The author(s) disclosed receipt of the following financial support for the research, authorship, and/or publication of this article: The study was in part supported by GE Healthcare.

References

1. Siegel RL, Miller KD, Jemal A. Cancer statistics, 2016. *CA Cancer J Clin*. 2016;66(1):7–30.
2. Muller BG, Shih JH, Sankineni S, et al. Prostate cancer: interobserver agreement and accuracy with the revised prostate imaging reporting and data system at multiparametric MR imaging. *Radiology*. 2015;277(3):741–750.
3. Jadvar H. Prostate cancer: PET with 18F-FDG, 18F- or 11C-acetate, and 18F- or 11C-choline. *J Nucl Med*. 2011;52(1):81–89.
4. Umbehr MH, Muntener M, Hany T, Sulser T, Bachmann LM. The role of 11C-choline and 18F-fluorocholine positron emission tomography (PET) and PET/CT in prostate cancer: a systematic review and meta-analysis. *Eur urol*. 2013;64(1):106–117.
5. Rauscher I, Maurer T, Fendler WP, Sommer WH, Schwaiger M, Eiber M. (68)Ga-PSMA ligand PET/CT in patients with prostate cancer: how we review and report. *Cancer Imaging*. 2016;16(1):14.
6. Lindenberg L, Ahlman M, Turkbey B, Mena E, Choyke P. Evaluation of prostate cancer with PET/MRI. *J Nucl Med*. 2016; 57(suppl 3):111S–116S.
7. Lee MS, Cho JY, Kim SY, et al. Diagnostic value of integrated PET/MRI for detection and localization of prostate cancer: comparative study of multiparametric MRI and PET/CT. *J Magn Reson Imaging*. 2017;45(2):597–609.
8. Hausmann D, Bittencourt LK, Attenberger UI, et al. Diagnostic accuracy of 18F choline PET/CT using time-of-flight reconstruction algorithm in prostate cancer patients with biochemical recurrence. *Clin Nucl Med*. 2014;39(3):e197–e201.
9. Karp JS, Surti S, Daube-Witherspoon ME, Muehllehner G. Benefit of time-of-flight in PET: experimental and clinical results. *J Nucl Med*. 2008;49(3):462–470.
10. Surti S, Karp JS, Popescu LM, Daube-Witherspoon ME, Werner M. Investigation of time-of-flight benefit for fully 3-D PET. *IEEE Trans Med Imaging*. 2006;25(5):529–538.
11. Minamimoto R, Levin C, Jamali M, et al. Improvements in PET image quality in time of flight (TOF) simultaneous PET/MRI. *Mol Imaging Biol*. 2016;18(5):776–781.
12. Iagaru A, Mittra E, Minamimoto R, et al. Simultaneous whole-body time-of-flight 18F-FDG PET/MRI: a pilot study comparing SUVmax with PET/CT and assessment of MR image quality. *Clin Nucl Med*. 2015;40(1):1–8.
13. Surti S. Update on time-of-flight PET imaging. *J Nucl Med*. 2015; 56(1):98–105.
14. Herzog H, Lerche C. Advances in clinical PET/MRI instrumentation. *PET clin*. 2016;11(2):95–103.
15. Hu Z, Yang W, Liu H, et al. From PET/CT to PET/MRI: advances in instrumentation and clinical applications. *Mol Pharm*. 2014; 11(11):3798–3809.
16. Choi JY, Yang J, Noworolski SM, et al. 18F Fluorocholine dynamic time-of-flight PET/MR imaging in patients with newly diagnosed intermediate- to high-risk prostate cancer: initial clinical-pathologic comparisons. *Radiology*. 2017;282(2): 429–436.
17. Teoh EJ, McGowan DR, Macpherson RE, Bradley KM, Gleeson FV. Phantom and clinical evaluation of the Bayesian penalized likelihood reconstruction algorithm Q.Clear on an LYSO PET/CT system. *J Nucl Med*. 2015;56(9):1447–1452.
18. Lantos J, Iagaru A, Levin C. Standard OSEM vs. Q.Clear® PET image reconstruction: an analysis of phantom data. *J Nucl Med*. 2015;56(suppl 3):264.
19. Ahn S, Ross SG, Asma E, et al. Quantitative comparison of OSEM and penalized likelihood image reconstruction using relative difference penalties for clinical PET. *Phys Med Biol*. 2015; 60(15):5733–5751.
20. Wangerin KA, Ahn S, Wollenweber S, et al. Evaluation of lesion detectability in positron emission tomography when using a convergent penalized likelihood image reconstruction method. *J Med Imaging (Bellingham)*. 2017;4(1):011002.
21. Fendler WP, Schmidt DF, Wenter V, et al. 68Ga-PSMA-HBED-CC PET/CT detects location and extent of primary prostate cancer. *J Nucl Med*. 2016;57(11):1720–1725.
22. Cooperberg MR, Pasta DJ, Elkin EP, et al. The University of California, San Francisco Cancer of the Prostate Risk Assessment score: a straightforward and reliable preoperative predictor of disease recurrence after radical prostatectomy. *J Urol*. 2005; 173(6):1938–1942.
23. Cooperberg MR, Broering JM, Carroll PR. Risk assessment for prostate cancer metastasis and mortality at the time of diagnosis. *J Natl Cancer Inst*. 2009;101(12):878–887.
24. Vanderhoek M, Perlman SB, Jeraj R. Impact of the definition of peak standardized uptake value on quantification of treatment response. *J Nucl Med*. 2012;53(1):4–11.

25. Kadrmas DJ, Casey ME, Conti M, Jakoby BW, Lois C, Townsend DW. Impact of time-of-flight on PET tumor detection. *J Nucl Med*. 2009;50(8):1315–1323.
26. Lois C, Jakoby BW, Long MJ, et al. An assessment of the impact of incorporating time-of-flight information into clinical PET/CT imaging. *J Nucl Med*. 2010;51(2):237–245.
27. El Fakhri G, Surti S, Trott CM, Scheuermann J, Karp JS. Improvement in lesion detection with whole-body oncologic time-of-flight PET. *J Nucl Med*. 2011;52(3):347–353.
28. Jakoby BW, Bercier Y, Conti M, Casey ME, Bendriem B, Townsend DW. Physical and clinical performance of the mCT time-of-flight PET/CT scanner. *Phys Med Biol*. 2011;56(8): 2375–2389.
29. Sampaio Vieira T, Borges Faria D, Azevedo Silva F, Pimentel F, Pereira de Oliveira J. The impact of a Bayesian penalized likelihood reconstruction algorithm on the evaluation of indeterminate pulmonary nodules by dual-time point 18F-FDG PET/CT. *Clin Nucl Med*. 2017;42(7):e352–e354.